BYOUNGJUN JEON*, SEONG HO SOHN*, WONSIK LEE*, CHULWOONG HAN *, YOUNG DO KIM**, HANSHIN CHOI*,♯

DOUBLE STEP SINTERING BEHAVIOR OF 316L NANOPARTICLE DISPERSED MICRO-SPHERE POWDER

DWUETAPOWE SPIEKANIE MIKROSFERYCZNYCH NANOCZĄSTEK PROSZKU 316L

316L stainless steel is a well-established engineering material and lots of components are fabricated by either ingot metallurgy or powder metallurgy. From the viewpoints of material properties and process versatility, powder metallurgy has been widely applied in industries. Generally, stainless steel powders are prepared by atomization processes and powder characteristics, compaction ability, and sinterability are quite different according to the powder preparation process. In the present study, a nanoparticle dispersed micro-sphere powder is synthesized by pulse wire explosion of 316L stainless steel wire in order to facilitate compaction ability and sintering ability. Nanoparticles which are deposited on the surface of micro-powder are advantageous for a rigid die compaction while spherical micro-powder is not to be compacted. Additionally, double step sintering behavior is observed for the powder in the dilatometry of cylindrical compact body. Earlier shrinkage peak comes from the sintering of nanoparticle and later one results from the micro-powder sintering. Microstructure as well as phase composition of the sintered body is investigated.

Keywords: 316L stainless steel, nanoparticle dispersed micro-sphere, pulse wire explosion, sintering

1. Introduction

Near net shaping in components manufacturing has taken advantages on material utilization efficiency, economic benefits, and effective production. As a matter of fact, powder metallurgy shows improved buy-to-fly ratio with facile production for complex components fabrication when it is compared to conventional subtractive manufacturing that is based on casting and machining [1-4]. Powders such as blended elemental powders and pre-alloyed powders are compacted and then sintered in the conventional powder metallurgy. Powder characteristics have crucial influences on compaction behavior, sintering behavior, and product properties [5,6]. Powder characteristics can be divided into primary factors and secondary factors. Primary factors are intrinsic material properties such as mechanical properties, thermo-physical properties, and so forth. Meanwhile, morphology, size, and size distribution are secondary factors which depends on powder production technology [7,8]. When a certain material is selected for powder metallurgy, processing ability is determined by secondary powder characteristics. Morphology may be a representative example. Spherical powder results in higher packing density than irregular counterpart. However, it is more difficult to be compacted. Inhomogeneous pore size and distribution of irregular powder compact are drawbacks in the sintering stage though interlocking between irregular powders is beneficial for compaction. Accordingly, compaction ability and

sintering ability are compromised from the viewpoint of manufacturing strategy. On the other hand, powder size is another important factor in the powder metallurgy. With powder size reducing, compaction ability becomes difficult but enhanced sinterability is facilitated [9-12]. In the extreme, sintering behaviors of nanoparticle are quite different from the conventional micro-powder owing to large surface-to-volume ratio. Nevertheless, extremely low packing density and compaction ability are challenges to be overcome aside from cost. In these contexts, other approaches to facilitate compaction and sintering are explored to meet the industrial requirements. Blended powders of nanoparticle and micro-powder can be a third option in the powder metallurgy. In the previous study [13], tungsten nanoparticle attached micro-powder showed higher density than conventional micro-powder in the spark plasma sintering. Especially, sintering kinetics is much enhanced at low temperature by the added nanoparticle [11]. Meanwhile, feedstock powder was prepared by mechanical blending nanoparticle with micro-powder. It needs multiple steps for powder preparation and dispersion uniformity without contamination is challenging. Accordingly, in-situ synthesis of nanoparticle attached micro-powder is beneficial from the engineering point of view. In the present study, 316L stainless steel nanoparticle dispersed micro-powder is synthesized by wire pulse explosion which belongs to vapor phase condensation. Nanoparticle dispersed micro-powder is in-situ synthe-

*   INCHEON REGIONAL DIVISION, KOREA INSTITUTE OF INDUSTRIAL TECHNOLOGY, INCHEON 406-840, SOUTH KOREA
**   HANYANG UNIVERSITY, SEOUL 133-791, SOUTH KOREA
♯   Corresponding author: hschoi@kitech.re.kr

sized by intentionally changing process window to suppress vaporization degree. Linear shrinkage behavior of nanoparticle and micro-powder blended powder is investigated using dilatometry and microstructures are observed.

2. Experimental

316L stainless powder was prepared by pulse wire explosion process and the experimental parameters are summarized in Table 1. Dissimilar to general nanoparticle synthesis in pulse wire explosion process, relatively thick wire is exploded in an inert gas environment. As-synthesized powder was characterized by x-ray diffractometry and electron spectroscopy with energy dispersion spectrometry. In addition, nanoparticles were detached from as-synthesized powder by ultrasonic treatment in ethyl alcohol and they were filtered to separate fine particle from coarse one. After ultrasonic detachment and filtering, coarse micro-powder is designated as underlying micro-powder while detached powder is named as surface fine powder.

TABLE 1

Pulse wire explosion process parameters for 316L stainless steel powder preparation

Applied voltage	Gas-atm	Wire length	Wire diameter	Feed speed	Straight speed
25kV	N2-200	100 mm	0.4 mm	25 mm/min	41.6 mm/sec

Linear shrinkage behaviors of the synthesized powder and surface fine powder were investigated by high temperature dilatometry. To do this, as-received powder and surface fine powder were cold compacted by a rigid mold under the uniaxial pressure of 400 MPa. After that, the cold compacts were heated to sintering temperature of 1.300°C at the heating rate of $5°C·min^{-1}$ in reducing environment. Sintering time was 180 minutes and then it was furnace cooled to room temperature. After dilatometry, microstructures of the sintered bodies were investigated by scanning electron microscopy and transmission electron microscopy.

3. Results and discussion

Morphologies of as-synthesized 316L stainless steel powder, coarse micro-powder, and surface fine powder are shown in Fig. 1. As-synthesized powder shows coarse and irregular morphology and the surface is covered with fine particle to form porous layer as shown in Fig. 1 (a). Representative cross-sectional microstructure is shown in Fig. 1 (b). Spherical and solid micro-powder is cored and fine particles are attached on the surface. In some cases, fine micro-powders and submicron powders are blended together as designated as [A] in Fig. 1 (b). After ultrasonic treatment and filtering, surface fine powders are effectively detached from cored micro-powder. Both coarse micro-powder and surface fine powder prominently reveals that nanoparticle and fine micro-powder are attached on the coarse micro-powder. During the pulse wire explosion process, pulse current passes through the wire feedstock and

accordingly, wire is heated by Joule heating [14]. Rapid heating results in inhomogeneous phase transformation of wire feedstock of liquid, gas, and plasma [15]. Finally, heated wire is exploded. Accordingly, liquid droplet and vapor species are generated and they undergo different reaction pathways during cooling. Liquid droplet is spheroidized in order to reduce surface energy and it is solidified to spherical micro-powder. On the other hand, nanoparticle is nucleated and grown via super-saturation during cooling. In-flight particles collide each other during flight and accordingly, agglomerations between nanoparticles and between nanoparticle and micro-powder occurs [16]. As a result, nanoparticle attached micro-powder can be obtained. It is difficult to quantify the particle size and size distribution though weight fraction of coarse micro-powder in the as-received powder was 15 wt.%. Qualitatively, surface fine powder is considered to have higher fraction of nanoparticle than as-received one.

(a) Plan-view morphology of as-synthesized powder

(b) Cross-sectional morphology of (a)

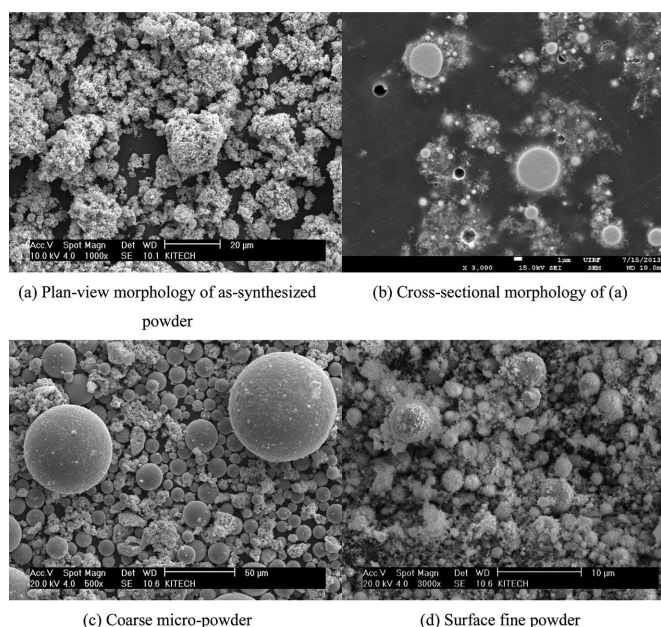(c) Coarse micro-powder

(d) Surface fine powder

Fig. 1. Morphologies of as-synthesized 316L stainless steel powder, coarse micro-powder, and surface fine powder. Coarse micro-powder and surface fine powder are obtained from ultrasonic detachment of the synthesized powder: (a) Plan-view morphology of as-synthesized powder, (b) Cross-sectional morphology of (a), (c) Coarse micro-powder and (d) Surface fine powder

Linear shrinkage behaviors of the powders are shown in Fig. 2. In association with thermal cycle, it is divided into heating, isothermal holding, and cooling stages. During heating stage, compact bodies undergo thermal expansion and then they shrink by sintering. In general, commercial micro-powder shows a monotonous linear shrinkage behavior during high temperature dilatometry [17]. However, it is prominent that nanoparticle dispersed micro-powders show a step-wise sintering behavior which consists of the first shrinkage at low temperature and following second shrinkage at relatively high temperature. This kind of step-wise sintering is defined as double step sintering in the present study. Another characteristics in linear shrinkage of nanoparticle attached micro-powder is the presence of intermittent period between the first shrinkage step and the second one. It implies that the sintering mechanism of lower temperature is different from that of higher

temperature. Onset temperature of the first shrinkage step is about 530°C and that of the second shrinkage step starts about 830°C for both powders. When they are compared to the commercial micro-powder, even onset point of the second shrinkage is significantly lower than commercial micro-powder of which onset point is about 1.050°C. Sintering temperature is largely dependent on the particle size. As the particle size is decreased, specific surface area is increased. It is prominent for nanoparticle. As a result, surface energy which is the driving force for sintering is much enhanced when nanoparticles are added for solid state sintering. Thermally activated mass transport is also facilitated as is expected from the Laplace equation in association with sinter stress. Therefore, surface diffusion, grain boundary diffusion, and volume diffusion in the nanoparticle dispersed micro-granule are activated at lower temperature than micro-powder [18]. However, sintering accompanies particle growth and therefore particle growth consumes driving force. In accordance with particle growth, further densification is driven by sintering of micro-powder. It is believed for the double step sintering in nanoparticle attached micro-powder. After that, they shrink slightly during isothermal holding: 0.2% for the synthesized powder and 0.27% for the surface fine powder. During cooling, linear shrinkage curves of as-synthesized powder and surface fine powder show linearity and the mean thermal expansion coefficients of them are 18.2×10^{-6} and 17.8×10^{-6} K^{-1}, respectively. They correspond to γ-austenite phase. Accordingly, it means that homogenization of chemical composition occurs during heat treatment. Surface fine particle which has higher nanoparticle fraction shows a larger shrinkage after dilatometry than as-synthesized one. It results from the lower green density of cold compact body: green density of surface fine powder was 74.0% and that of as-synthesized powder was 77.3% after 400 MPa compaction.
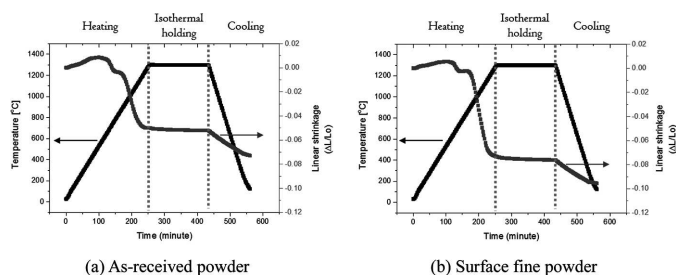

Fig. 2. Linear shrinkage behaviors of as-synthesized 316L stainless steel powder and surface fine powder: (a) As-received powder and (b) Surface fine powder

Figure 3 shows back-scattered electron photographs: cross-sectional microstructures of as-synthesized powder and surface fine powder after the heat treatment. Seemingly, sintered body is surrounded by dense outer region [A] without any defective microstructures while dispersoids are dispersed in inner region [B], regardless of the powders. The dispersoids look like pore but they are particulate phases. When both powder morphologies and sintered body microstructures are taken into consideration, particulate phases are present along the micro-powder boundaries such as triple junction boundary where final densification occurs. Particulate phases are closely investigated according to the position. Figure 3 (c) shows representative microstructures adjacent to the interface between

dense outer region [A] and inner region [B]. Elongated and spherical particulate phases [II] are dispersed in the matrix [I]. They has smooth interface with matrix. In the case of inner region of Fig. 3 (d), facet particles [III] are contrasted to smooth particles [II]: facet particles are of gray color while smooth particles are black in the back scattered electron image in which chemical composition differences make difference in contrast. It is worthwhile to note that particle size is larger but particle frequency is lower near the interfacial region between dense outer region (A) and inner region as it can be compared from Fig. 3 (c) and (d). Besides, particulate population of sintered body from surface fine powder is notably higher than that of sintered body from as-synthesized powder. The difference between them is related to powder characteristics, especially for nanoparticle and fine micro-powder fraction.
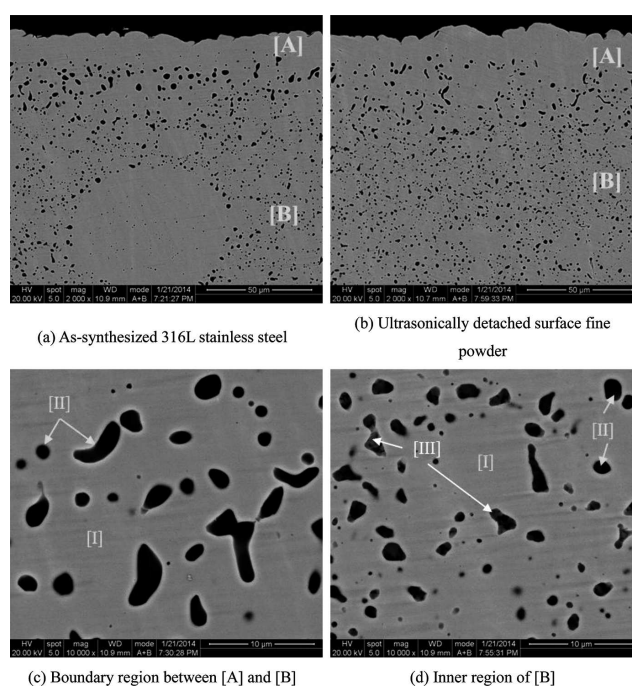

Fig. 3. Microstructures of heat treated 316L stainless steel bodies from as-synthesized powder and surface fine powder: [A] is the continuous outer dense region and [B] is inner region with oxide dispersoids: (a) As-synthesized 316L stainless steel, (b) Ultrasonically detached surface fine powder, (c) Boundary region between [A] and [B] and (d) Inner region of [B]
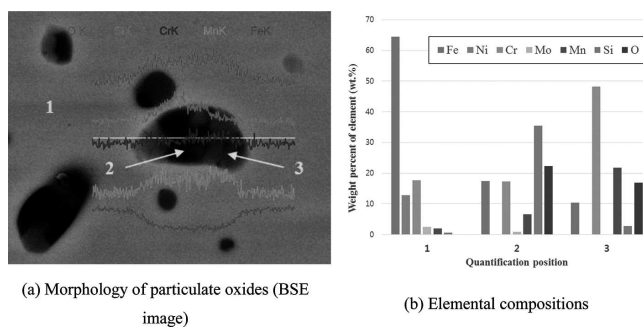

Fig. 4. SiO_2 and $MnCr_2O_4$ oxides dispersed in the sintered body: matrix is marked 1, black particle is marked 2, and gray particle is marked 3 and elemental compositions of (b) comes from point quantification of each region: (a) Morphology of particulate oxides (BSE image), (b) Elemental compositions

Chemical compositions of the particulate phases were further investigated. Figure 4 shows elemental distributions in which black particle borders gray particles. Black and gray particles are dispersed in matrix (1). Elemental line distribution reveals that the particulate dispersoids are oxides. Si is rich in black particles while Mn and Cr are enriched in gray particles. It is further confirmed by the point quantification result of Fig. 4 (b). In our other study, it was proven that Si rich black particle is SiO_2 and Cr-Mn rich gray particle is $MnCr_2O_4$. $MnCr_2O_4$ comes into contact with SiO_2. Areal fraction of oxide was measured in the inner region for each sintered body: surface fine powder was 18.0% and as-received powder was 13.2%. Higher oxide phase fraction of surface fine powder result from the higher phase fraction of nanoparticle which is susceptible for air oxidation.

4. Conclusions

In order to verify the effects of nanoparticle addition to the micro-powder on the sintering behavior, nanoparticle dispersed micro-powder was synthesized and sintering behavior was investigated by high temperature dilatometry.

1. Nanoparticle dispersed microsphere 316L stainless steel powder is obtained from pulse wire explosion of 316L stainless steel wire in the inert gas environment. During the process, exploding wire undergoes two different reaction pathways: atomization and solidification pathway and vaporization and condensation pathway. The former reaction results in the spheroidized micro-powder while nanoparticle is synthesized by the latter reaction pathway. Nanoparticles are deposited on the micro-powder surface through the collision between in-flight micro-powders and nanoparticles.

2. Owing to the differential thermo-physical properties of alloying elements, inhomogeneous phase composition and chemical composition result from elemental redistribution during the pulse wire explosion process.

3. Linear shrinkage behavior of the cold compact from the powder demonstrates that nanoparticle has an influence on sintering behavior. Nanoparticle dispersed micro-powder shows a double step sintering behavior. First stage at low temperature results from the sintering of nanoparticle and however, final densification is achieved by the sintering of micro-powder in the athermal sintering. The lower temperature sintering results from the enhanced sintering ability of nanoparticle.

4. After the dilatometry, chemical composition is homogenized by elemental diffusion during sintering. SiO_2 and $MnCr_2O_4$ oxides are stably present in the sintered bodies.

REFERENCES

[1] R.E.D. Mann, R.L. Hexemer Jr, I.W. Donaldson, D.P. Bishop, Mater. Sci. Eng. **525**, 5776 (2011).

[2] R. Baccino, F. Moret, F. Pellerin, D. Guichard, G. Raisson, Mater. Des. **21**, 345 (2000).

[3] Yoshinobu, Takeda, J. Kor. Powd. Met. Inst. **5**, 340 (1998).

[4] B. Kieback, G. Stephani, T. Weibgarber, T. Schuberrt, U. Waag, A. Bohm, O. Andersen, M. Gohler, M. Reinfried, J. Kor. Powd. Met. Inst. **10**, 383 (2003).

[5] B.P Saha, V. Kumar, S.V. Joshi, A. Balakrishnan, C.L. Martin, Powder Technol. **224**, 90 (2012).

[6] J.M. Ting, R.Y. Lin, J. Mater. Sci. **30**, 2382 (1995).

[7] H.S. Kim, Y.Y. Kim, D.K. Park, I.S. Ahn, J. Kor. Powd. Met. Inst. **20**, 203 (2013).

[8] L.E. Euliss, J.A. DuPont, S. Gratton, J. DeSimone, Chem. Soc. Rev. **35**, 1095 (2006).

[9] S. Patel, A.M. Kaushal, A.K. Bansal, Pharm. Res. **24**, 111 (2006).

[10] K. Komeya, H. Inoue, J. Mater. Sci. **4**, 1045 (1969).

[11] M.J. Kirchhof, H. Forster, H.J. Schmid, W. Peukert, J. Aerosol Sci. **45**, 26 (2012).

[12] L. Jiang, Y. Liao, Q. Wan, W. Li, J. Mater. Sci. – Mater. Med. **22**, 2429 (2011).

[13] H.S. Joo, C.W. Han, B.M. Kim, D.H. Kim, H.S. Choi, Rev.Adv. Mater. Sci. **28**, 200 (2011).

[14] R. Sarathia, T.K. Sindhu, S.R. Chakravarthy, Archana Sharmac, K.V. Nageshc, J. Alloys Compd. **475**, 658 (2009).

[15] J.K. Antony, N.J. Vasa, S.R. Chakravarthy, R. Sarathi, J. Quant, Spectrosc. Radiat. Transfer **111**, 2509 (2010).

[16] S. Krishnan, A.S.M.A. Haseeb, M.R. Johan, J. Nanopart. Res. **15**, 1 (2013).

[17] A.S. Nykiel, M. Nykiel, Arch. Foundry Eng. Special Issue **3**, 235 (2010).

[18] W. Zhang, I. Gladwell, Int. J. Comput. Mater. Sci. Surf. Eng. **12**, 84 (1998).